INTERFACE

rsif.royalsocietypublishing.org

Research

**Cite this article:** Zhang S, Bassett DS, Winkelstein BA. 2016 Stretch-induced network reconfiguration of collagen fibres in the human facet capsular ligament. *J. R. Soc. Interface* **13**: 20150883.
http://dx.doi.org/10.1098/rsif.2015.0883

Received: 8 October 2015
Accepted: 7 January 2016

**Subject Areas:**
bioengineering, biomechanics, mathematical physics

**Keywords:**
collagen, fibre realignment, facet capsular ligament, community detection, time-dependent network

**Author for correspondence:**
Beth A. Winkelstein
e-mail: winkelst@seas.upenn.edu

†These authors contributed equally to this study.

Electronic supplementary material is available at http://dx.doi.org/10.1098/rsif.2015.0883 or via http://rsif.royalsocietypublishing.org.

THE ROYAL SOCIETY PUBLISHING

# Stretch-induced network reconfiguration of collagen fibres in the human facet capsular ligament

Sijia Zhang[1], Danielle S. Bassett[1,2,†] and Beth A. Winkelstein[1,3,†]

[1]Department of Bioengineering, [2]Department of Electrical and Systems Engineering, and [3]Department of Neurosurgery, University of Pennsylvania, Philadelphia, PA 19104, USA

Biomaterials can display complex spatial patterns of cellular responses to external forces. Revealing and predicting the role of these patterns in material failure require an understanding of the statistical dependencies between spatially distributed changes in a cell's local biomechanical environment, including altered collagen fibre kinematics in the extracellular matrix. Here, we develop and apply a novel extension of network science methods to investigate how excessive tensile stretch of the human cervical facet capsular ligament (FCL), a common source of chronic neck pain, affects the local reorganization of collagen fibres. We define collagen alignment networks based on similarity in fibre alignment angles measured by quantitative polarized light imaging. We quantify the reorganization of these networks following macroscopic loading by describing the dynamic reconfiguration of network communities, regions of the material that display similar fibre alignment angles. Alterations in community structure occur smoothly over time, indicating coordinated adaptation of fibres to loading. Moreover, flexibility, a measure of network reconfiguration, tracks the loss of FCL's mechanical integrity at the onset of anomalous realignment (AR) and regions of AR display altered community structure. These findings use novel network-based techniques to explain abnormal collagen fibre reorganization, a dynamic and coordinated multivariate process underlying tissue failure.

## 1. Introduction

The structural integrity of biomaterials depends on complex interactions between the individual material components and their surroundings. At the extreme of the loss of such integrity, the tissue can fail, but the more subtle tissue responses that occur in the macroscopic subfailure regime are also critical in the pathomechanisms of physiological dysfunction. The cervical facet capsular ligament (FCL) is a quintessential example material in which the subfailure tissue responses have an important physiological impact, even in the absence of macrostructural failure. The FCL is innervated by nociceptive neurons that are responsible for pain sensation [1–3]. Excessive FCL stretch, which can occur during neck trauma, can activate the nociceptive pain fibres embedded in the collagen matrix of the FCL [1,3,4]. The mechanisms by which FCL stretch induces pain are believed to depend on the kinematics and kinetics of the local collagen fibre matrix, which under normal physiological circumstances, can accommodate macroscopic tissue deformations via local fibre motion and matrix reorganization [5–7]. However, some FCL loading conditions can result in collagen disorganization and microstructural injury [4–6,8]. Despite growing evidence supporting this notion, collagen fibre kinematics during FCL loading and the ability to predict the relationships between those responses and tissue injury are still not well understood.

The reconfiguration of collagen fibres during FCL loading can be characterized as either normal or anomalous. Anomalous collagen fibre realignment occurs when local fibre directions change significantly more than expected in the majority of the tissue, redistributing forces after the load-bearing fibres have

failed [5,6]. Anomalous fibre realignment is an important predictor of tissue injury; it is associated with the occurrence of altered mechanical properties, occurs prior to any visual signs of tissue rupture [5,6] and predicts the location of eventual tissue failure [5,6,8]. Fibre realignment during loading has been measured empirically using dynamic quantitative polarized light imaging (QPLI) to generate a sequence of spatial maps of collagen fibre alignment over time [6,8,9]. Prior studies have demonstrated the feasibility of using QPLI to accurately assess collagen fibre alignment in human cervical FCLs [5,8,10–12]. The correlations between alignment vectors over time have previously been used to define regions of anomalous fibre realignment, which enables accurate quantitative and spatial measurements of changes in collagen fibre orientation [5]. Yet, this detection technique and existing image-based computer models capture tissue damage at the single pixel or fibre level [5,7,8], and so remain naive to any larger-scale collective realignment of fibre *groups* as they adapt to FCL loading. As such, it is not known if, and to what extent, the collagen matrix displays spatially extended domains whose changes during macroscopic loading may affect, or relate to, the mechanical behaviour of ligamentous tissues. Understanding changes in mesoscale collagen fibre networks can improve the detection and prediction of local tissue failure, because the eventual rupture of collagenous tissue involves damage to collagen fibre bundles and/or a large number of distributed collagen fibres in domains greater than several fibres in the microscale [13–15].

The understanding of collagen realignment has been hampered by the lack of analytical methods to probe the collective *coordination* of realignment across many spatially distributed fibres. Here we suggest that the complexity of this coordinated multivariate process can be successfully captured using tools from the field of network science [16]. Networks provide a useful representational framework to systematically examine the topological characteristics and the dynamics of complex systems [17–19]. System components are represented as network nodes and their relationships with one another are represented as network edges [20,21]. In many biological [19,22,23] and material [24,25] systems, this formalism reveals important organizational changes that impact the system's underlying structure and resulting function. For example, network-based tools known as *community detection techniques* can be used to characterize the presence and organization of local geographical domains in non-biological materials [24–26] which are referred to as network communities or modules. These domains constrain sensitivity to mechanical perturbations in the form of acoustic signals [24] and track alterations in material topology as a function of applied force (pressure) [25], indicating their broad sensitivity to material microstructure.

Here, we investigated the effects of the stretch-induced microscopic fibre movements on the mesoscale organization of local collagen networks in relation to FCL mechanics using tools from network science. We defined collagen networks based on the similarity in fibre alignment directions acquired using QPLI during FCL loading, and applied novel community detection techniques [27] to probe organizational changes that may be due to anomalous realignment (AR) of fibres. We summarized the temporal evolution of the networks using diagnostics such as modularity (which measures the presence and strength of time-dependent communities) and flexibility (which measures the reconfiguration of communities) [27,28]. We then compared dynamic properties of the network architecture between regions with AR and regions with normal realignment (NR) in the FCL, and investigated their associations with macroscopic tissue mechanics. We hypothesized that regions with AR are associated with greater changes in the collagen network structure than regions with NR, and that network disorganization contributes to the loss of tissue mechanical integrity, both of which are detectable using the community detection technique. The successful implementation of these graph-theoretic techniques on collagen networks can have broader impact in quantifying the organization and defining the structure–function relationships of other fibrous connective tissues and heterogeneous materials.

## 2. Material and methods

### 2.1. Collagen alignment and macromechanics in human facet capsular ligament tissue

Collagen fibre alignment data and mechanical data of the human cervical FCLs were obtained previously during loading using a system that integrates QPLI with a tensile testing device [5]. In this study, we included only those specimens ($n = 7$; age $63 \pm 15$ years; two females) in which AR was detected with sufficient light transmission by a previously defined vector correlation analysis [5]. Briefly, the central region of the ligament surface of each human C4/C5 FCL sample was labelled with a grid of fiduciary markers dividing it into subregions (figure 1*a*). QPLI data were acquired with a 12.5 pixel $mm^{-1}$ resolution in the unloaded reference position with the ligament under 5 kPa of pre-stress, and also during continuously applied uniaxial tensile distraction until tissue failure. Continuous collagen fibre alignment maps were generated at 0.04 s increments. Both the forces and displacements during tensile loading were acquired at 1 kHz by an Instron testing machine and its Bluehill software (Instron Corporation, Norwood, MA). Stress was also measured for each specimen throughout loading using the recorded force data and that specimen's cross-sectional area when unloaded.

### 2.2. Network construction

For each specimen, we created two rectangular regions of interest (ROIs) including (i) a region with anomalous fibre realignment and (ii) one with normal realignment (figure 1*a*) based on previous work using similar regions as mesh elements for strain field calculations [5,8]. Tissue strains, such as the principal Lagrangian strains, have been used previously to define the response thresholds of soft tissues to external loading; strain thresholds have been defined for FCL's yield and failure, and for nociception from the FCL prior to visible tissue rupture [6,8,29–32]. However, most tissue strains measured in earlier studies are macroscopic and lack the resolution to detect microscopic tissue damage in subfailure conditions. Therefore, techniques that detect collagen fibre realignment have been developed to identify the majority of the mesh elements that sustain only the expected amount of fibre reorganization and a few regions that contain excessive collagen disorganization [5].

ROIs were selected based on those predetermined locations of normal and anomalous realignment that indicate microstructural tissue injury. The NR ROIs were chosen uniformly at random from the set of all normally realigned regions with sufficient, but not excessive, light transmission. Because fibre reorganization is the only criterion for the selection of ROIs, the group of normal realignment includes regions that are both adjacent to and distant from the anomalously realigned regions, and includes regions that both eventually developed visible rupture and regions that did not rupture. For anomalous realignment regions, we chose ROIs that exhibited the most anomalous realignment but did not sustain the maximum principal strain (MPS) of the ligament to

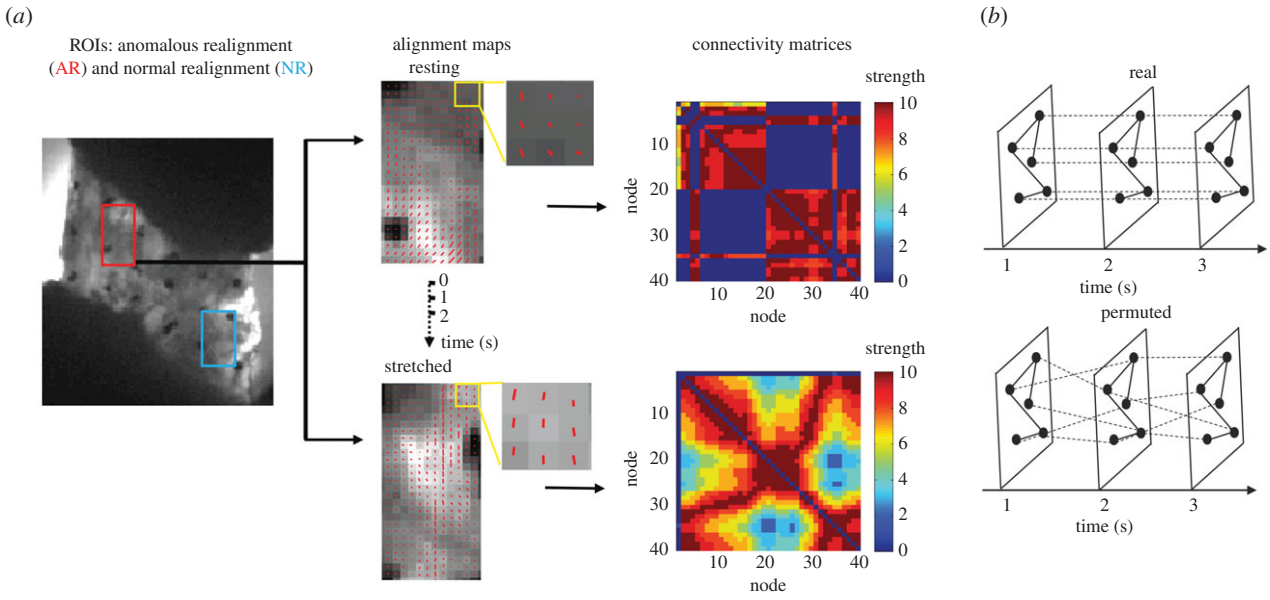


**Figure 1.** Network construction using QPLI data. (*a*) QPLI images obtained before and during loading were used to generate pixel-wise collagen alignment maps in the selected ROIs of anomalous realignment (AR; red box) and normal realignment (NR; blue box) at rest, at the onset of anomalous realignment, and in between those two time points at 1 s increments. Rectangular ROIs were defined using the upper left and lower right fiduciary markers as the common information between different time points. Network nodes were defined as 3 × 3 pixel windows in the ROIs at rest. Representative 3 × 3 pixel windows are shown at the resting and the stretched states, with corresponding demonstration of alignments. Network edges were established based on the difference in alignment angles between nodes. Weighted networks were constructed by thresholding and scoring the connection strength from 1 to 10. Connectivity matrices, with nodes numbered spatially, display the pairwise connectivity strength. (*b*) Schematic of multilayer networks in which consecutive time windows were connected by linking each node to itself for real networks (top) or linking nodes randomly to create permuted networks as nodal null models (bottom). (Online version in colour.)

represent collagen networks with the most detectable microscopic damage. Among all of the samples that we examined, only one of the 17 regions of anomalous fibre realignment overlapped with the location of the sample's MPS, suggesting a disconnection between tissue strain and fibre realignment measures [5]. Therefore, in order to decompose the effects of ligament strain and anomalous fibre realignment on tissue response to injurious loading, in this study, we evaluated only AR regions that displayed no co-localization with MPS.

Within each ROI, we generated fibre alignment maps using QPLI acquired at 1 s increments during the FCL distraction from the unloaded pre-stressed resting position to the stretched position at the onset of anomalous fibre realignment that was determined for that specimen (figure 1*a*). The nodes of the collagen networks were defined as non-overlapping 3 × 3 pixel windows in each ROI at the resting state, in order to decrease the sensitivity of the fibre orientation measurement to the random noise present at single pixels. Eight-pixel connectivity has been used to eliminate random noise when defining the occurrence of anomalous realignment [5]. In ROIs at the stretched positions, we defined network nodes based on the nodal configuration from the resting state. That is, we use the same number of nodes in each row and each column as in the resting position in order to generate networks with identical numbers of nodes before and during loading, a feature necessary for a fair comparison of network properties [33].

We defined the mean alignment direction in each window as the average of the fibre orientation angles within one standard deviation of all angles in that 3 × 3 pixel window. Using one standard deviation, we removed on average two pixels from the 3 × 3 pixel window that were farthest from the mean alignment direction. This approach minimized outliers [34] owing to fibre alignment measurement from aberrant pixels, but remained sensitive to the main alignment direction represented by a majority of fibres in each widow. Two nodes were considered 'connected' by a network edge if the difference in the mean alignment direction of the two nodes was less than 90°. We assigned integer weights to each edge from 1 (a difference of up to 100% of the 90°) to 10 (a difference of less than 10% of the 90°), such that smaller differences (greater similarity in mean alignment directions) weighed more (figure 1*a*). For instance, the edge between two nodes whose difference in mean alignment direction was smaller than 9° was given a weight of 10 (i.e. strongest connection), whereas the edge between two nodes whose difference in mean alignment direction was between 81° and 90° was given a weight of 1 (i.e. weakest connection). This integer weighting scheme is consistent with our confidence in the measured angles produced by the QPLI measurement, where a 9° polarizer step exists between each QPLI image collected during data acquisition [5,6,8].

## 2.3. Static community detection and network visualization

Our goal was to understand differences in the stretch-induced network organization in both regions of the FCL using networks measured in the unloaded condition in comparison with networks measured at the onset of anomalous fibre realignment in the FCL. To quantify network organization, we performed static community detection (a form of clustering for networks) by optimizing a modularity quality function [35] using a Louvain-like locally greedy algorithm [36]. In this approach, modules are defined as sets of nodes that are more highly interconnected than expected in an appropriate statistical null model [21,36]. The modularity index, which is optimized over different configurations that compartmentalize the network into modules, quantifies how well a network is segregated into modules (see appendix for mathematical details). Because of the near degeneracy of the modularity landscape [37], we optimized the modularity quality function 100 times and constructed a consensus partition for each network at the resting state and for each network at the onset of anomalous realignment, separately for both region types (AR and NR) in each specimen. To quantify how well the network was segregated into modules, we calculated the modularity using the consensus

partition for each state (resting and onset of anomalous realignment) and region (AR and NR). To determine the statistical significance of these modularity values, we constructed commonly used comparative benchmark networks by rewiring each collagen network 20 times while preserving (i) the number of nodes, (ii) the number of edges and (iii) the degree distribution (the *degree* of a node is defined by the number of connections emanating from that node). In this way, we constructed 100 benchmark null models and acquired an optimized modularity value from each null model. We computed the mean modularity over those 100 benchmark networks, and compared this value with that observed in the real network.

We visualized community structure in collagen networks using the software package MATLAB (R2014a, The MathWorks Inc., Natick, MA). The Fruchterman–Reingold algorithm [38] determined the placement of communities for each network, and the Kamada–Kawai algorithm [39] determined the location of nodes within a community [40].

## 2.4. Dynamic community detection and tissue mechanics

We next investigated the evolvability of the collagen network and its relationship to changes in the mechanical responses of the FCL during loading using dynamic community detection. We evaluated the dynamic modular structure on multilayer networks created by linking nodes between consecutive time steps [27] (figure 1*b*). Layers in the multilayer network represent time windows that are 1 s apart, starting from the baseline resting state and continuing through to the first detection of anomalous fibre realignment. In a multilayer network, identity links connect nodes in a given time window to themselves in the previous and subsequent time windows (figure 1*b*). We optimized the multilayer modularity index over partitions of nodes into communities over time [27]. After performing this optimization 100 times, we determined a consensus partition using the method outlined in reference [41]. To quantify statistical significance, we constructed 100 nodal null model networks for each real network by permuting the interlayer connections uniformly at random [28] (figure 1*b*). To describe the evolution of communities in collagen networks during loading, we calculated four diagnostics: the multilayer modularity index, the number of modules, stationarity [28] and flexibility [28] (see appendix for mathematical definitions). We compared the values of these four diagnostics estimated in the real networks to the mean values of the same diagnostics averaged over the set of 100 nodal null model networks constructed for each real network. We also assessed the differences in network diagnostics between the AR and NR regions to investigate the relationships between anomalous fibre realignment and dynamic properties of the community structure of the tissue.

To study the associations between dynamic features of the local collagen networks and tissue mechanics, we used linear regression to measure the correlations between the networks' flexibility and the forces and stresses generated in the tissue at the onset of anomalous realignment.

## 2.5. Software and statistics

All computations and statistical tests were performed using MATLAB and JMP (v. 11, SAS Institute). We implemented the network computations using a combination of the Brain Connectivity Toolbox [20], community detection code [42] and in-house software for stationarity, flexibility, consensus partitions and nodal null models [27,28].

We used paired *t*-tests to test the differences in modularity and the number of modules before and after stretch in AR and NR regions, and between real and randomized networks, both of which were further verified using non-parametric permutation tests. For the case of dynamic community detection on multilayer networks, we computed the differences in the four network diagnostics (modularity, number of modules, stationarity and flexibility) between real networks and nodal null models. We tested whether these differences were significantly different from zero using a one-sample *t*-test. Paired *t*-tests evaluated the differences in network diagnostics between the two regions of the FCL (AR and NR). Significance of the regression of FCL force and stress against flexibility was tested using an *f*-test. Significance was tested against $\alpha = 0.05$.

# 3. Results

We investigated changes in modular organization at the onset of anomalous fibre realignment in relation to the respective resting state. Anomalous realignment is defined as substantially more fibre reorganization of local collagen networks relative to the normal realignment and occurs to accommodate force redistribution caused by failure of the load-bearing fibres. Community detection was performed on four groups of weighted, undirected collagen fibre alignment networks, including AR regions at the resting and stretched states, and NR regions at the resting and stretched states. Networks of AR and NR regions had similar sizes: $39.4 \pm 7.4$ nodes and $39.7 \pm 4.5$ nodes, respectively; the two network sizes were not statistically different from one another ($p = 0.924$; $t = -0.099$) as tested using a two-sample *t*-test.

## 3.1. Static modular structure

We first evaluated collagen network reconfiguration at the onset of anomalous realignment with respect to the resting position in both regions with anomalous realignment and regions with normal realignment using community detection. Regions with anomalous fibre realignment exhibited heightened modular structure in the resting state compared with the state in which the ligament was stretched. Specifically, AR regions displayed decreases in both the modularity (paired one-tailed *t*-test: $p = 0.030$; $t = -2.284$) and the number of modules ($p = 0.015$; $t = -2.828$) after loading compared with rest (figure 2*a*). We observed no difference in NR regions after loading compared with rest (figure 2*b*). These results suggest that more robust collagen fibre reorientation altering the network architecture occurred during loading in regions sustaining more evident local fibre damage.

To test if the difference in AR regions between rest and the onset of anomalous fibre realignment was driven by node-level changes, we evaluated the relationships between node degree and modularity. We measured the unweighted node degree defined as the mean number of connections per node, and assessed the weighted node degree as a measure of the nodal connection strength. We found significant increases in the unweighted (paired one-tailed *t*-test: $p = 0.017$; $t = 2.732$) and weighted ($p = 0.007$; $t = 3.469$) node degrees at the onset of anomalous realignment with respect to rest in the anomalous realignment regions. Both the unweighted ($R = -0.471$; $p = 0.011$; $F = 7.41$; degree of freedom (d.f.) = 26) and the weighted ($R = -0.642$; $p = 0.0002$; $F = 18.2$; d.f. = 26) node degrees displayed significant negative correlations with modularity, as evident from *f*-tests (see also the electronic supplementary material, figure S1).

To further examine the contribution of the node degree to changes in the modular structure, we fixed the unweighted node degree of the stretched networks to be the same as

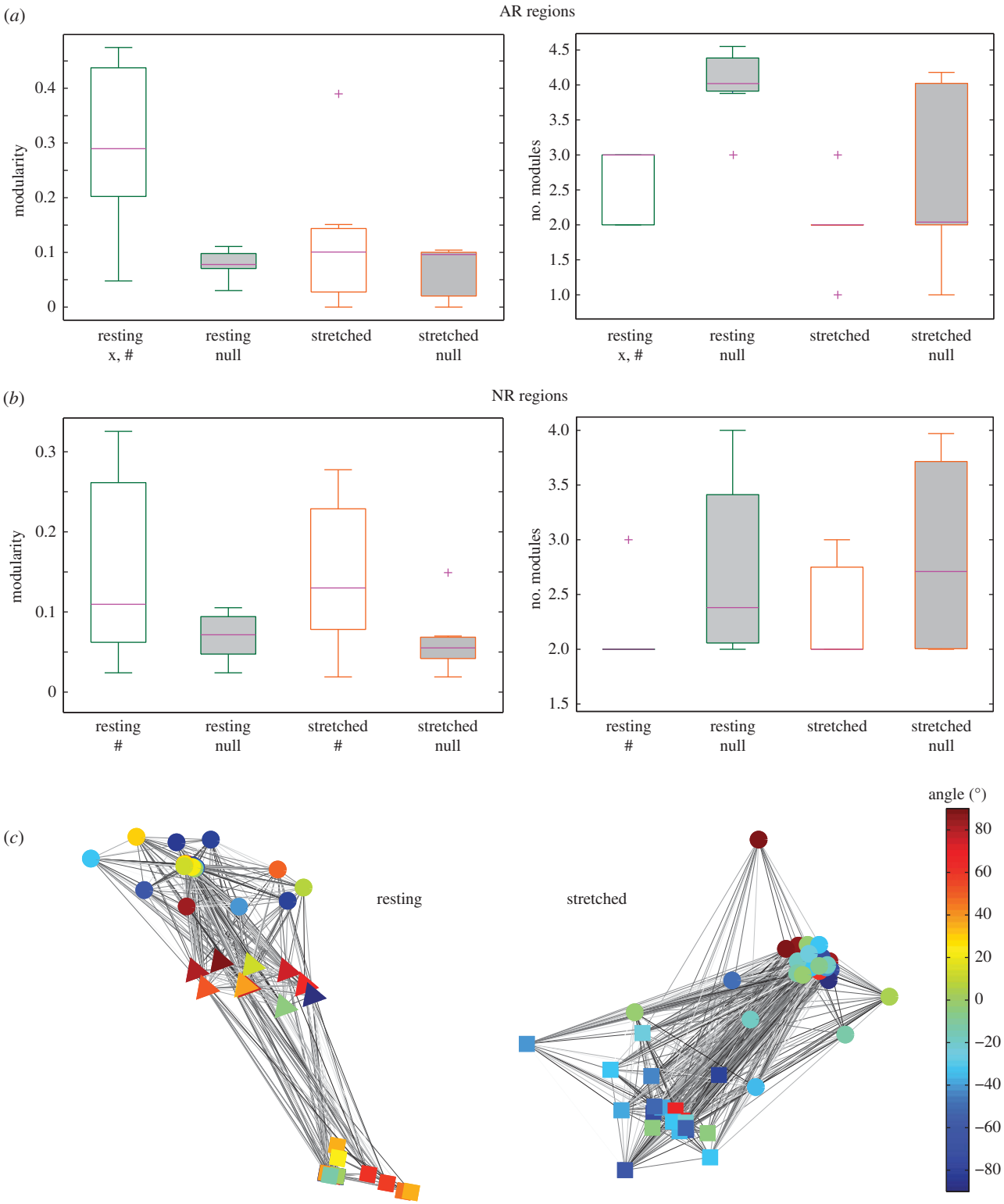


**Figure 2.** Static modular structures. (*a*) Modularity and the number of modules of collagen networks in regions with anomalous realignment (AR) showed significant changes from the non-random resting state (green boxes) to the random state at the onset of anomalous realignment (orange boxes), whereas (*b*) regions with normal realignment displayed no difference before (green boxes) and after (orange boxes) stretch. Below each boxplot, a single cross represents differences between rest and the onset of atypical realignment ($p < 0.031$); the hash sign (#) represents differences between real and randomized networks ($p < 0.035$). (*c*) Visualization of community structures of a representative region with anomalous fibre realignment. Force-directed placement of modules and nodes was used. Module assignment is indicated by node shape. Node colour shows the mean fibre alignment angle at a given node. The colour bar range is $-90^\circ$ to $90^\circ$. The number of modules and the mean fibre angle within each module of AR regions in all FCL samples are listed in electronic supplementary material, table S1. Edge strength is displayed in greyscale with black representing the maximum weight. (Online version in colour.)

that of the resting-state networks by preserving the strongest connections. As a result, we can no longer detect any statistical differences in modularity or weighted node degree between the resting and the stretched networks for either the AR or NR regions (electronic supplementary material, figure S2). These findings indicate that nodal-level changes play an important role in shaping the modular structure of the collagen network during FCL loading.

We next investigated whether the collagen network displayed any topological alterations from rest to the onset of

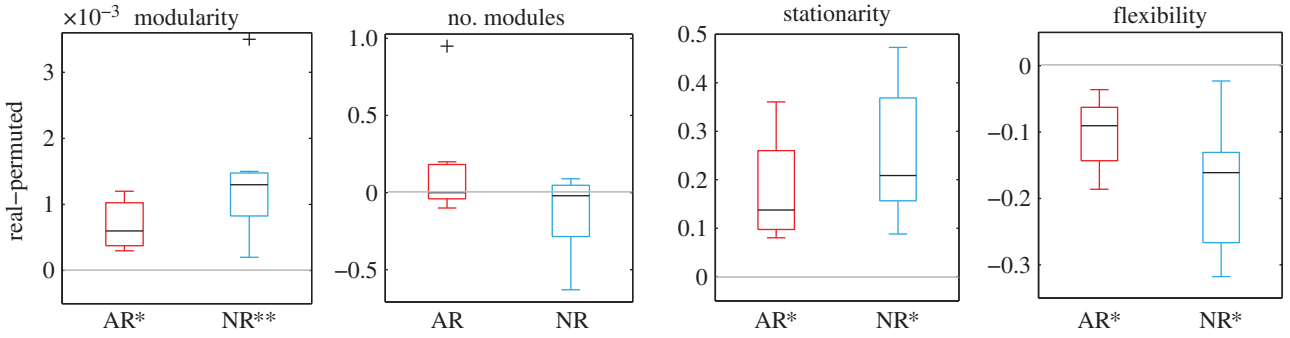


**Figure 3.** Network diagnostics of multilayer networks. Significant differences in modularity, stationarity and flexibility were found between real and permuted networks for both regions with and without anomalous realignment. No difference in the number of modules was detected. Asterisks are used below each plot to indicate significant differences from zero (grey line). A single asterisk indicates $p < 0.004$ and double asterisks indicate $p = 0.013$. (Online version in colour.)

anomalous realignment. We compared the network structure at rest and the onset of anomalous realignment in both the anomalous realignment and NR regions to their respective null model networks with the same node degree as the collagen network but otherwise random organization. Only anomalously realigned regions under stretch showed similar modularity and number of modules as null model networks, whereas the other three networks (AR region at rest, NR region at rest and NR region at the onset of anomalous realignment) exhibited significantly heightened ($p < 0.035$; $|t| > 2.205$) modular structure in comparison with null model networks as tested using paired one-tailed *t*-tests. The decreased modularity and the number of modules that were comparable to random levels in the anomalously realigned region after stretch was likely driven by an increase in the number of intermodular connections as the alignment directions became more similar between modules after loading (figure 2*c*). Because modules are defined as highly intraconnected clusters, increasing the intermodular links weakens the compartmentalization of the network into different communities and thus decreases the modularity. The shift in network structure observed in the AR regions from highly modular to random in comparison with null model networks with the same nodal degree suggests that complex topological alterations existed at the local network domain, which cannot be captured by single nodes or pixels.

## 3.2. Dynamic modular structure

We investigated how local collagen networks evolve and reorganize over time from rest to the onset of anomalous realignment by performing dynamic community detection on multilayer networks that represent the collagen network configuration at different time points. Dynamic community detection on multilayer networks revealed that the collagen network reorganized smoothly and adaptively over time. For both of the AR and NR regions, collagen fibre networks exhibited significantly higher modularity ($p < 0.013$; $t > 3.493$) than the null model as tested using one-sample *t*-tests (figure 3), indicating the presence of long-lasting modules that reflect coordinated fibre movements. In comparison with dynamic null model networks in both the AR and NR regions, we found a significant increase in stationarity, which measures the maintenance of nodal composition of modules over time (one-sample *t*-test: $p < 0.004$; $t > 4.671$); we also found a significant decrease in flexibility, which characterizes the altered nodal allegiance to modules, ($p < 0.004$; $t < -4.611$), indicating a smooth temporal transition between the resting and the stretched states (figure 3). We observed no difference in the number of modules between the real and null model networks (figure 3). Together, these findings suggest coordinated realignment of fibres to smoothly adapt to macroscopic ligament loading.

## 3.3. Regional differences in flexibility

To examine if, and how, dynamic features of local collagen network reconfiguration exhibit regional differences and play a role in modulating the macroscopic mechanical behaviours of the ligament, we tested for differences in the flexibility of AR and NR networks, and we evaluated relationships between FCL mechanics and network flexibility in both AR and NR regions. Differences in flexibility and its relationships to FCL mechanics were found in regions with and without anomalous realignment. Flexibility was significantly increased ($p = 0.029$; $t = 2.339$) in the AR regions compared with the NR regions in the same sample as tested by a paired one-tailed *t*-test (figure 4*a*). Significant correlations between the flexibility of the NR regions and each of the stress ($R = 0.890$; $p = 0.007$; $F = 19.1$; d.f. $= 5$) and force ($R = 0.877$; $p = 0.010$; $F = 16.6$; d.f. $= 5$) developed in the FCL were observed using linear regression with *f*-tests; whereas, although trending the same as the NR regions, AR regions showed no association between flexibility and either the FCL stress or force (figure 4*b*,*c*). Larger differences in flexibility between the AR and NR regions occurred in samples that produced lower stresses and forces at the onset of anomalous fibre realignment (figure 4*b*,*c*). These flexibility-related regional differences suggest that abnormal reorganization of collagen networks over time may contribute to the mechanical injury events that occur at the first detection of anomalous realignment, which were associated with the impaired mechanical integrity of the FCL.

# 4. Discussion

Collagen fibre realignment is a possible mechanism that transmits force from macroscopic FCL loading to deform and activate pain fibres embedded in the collagen matrix. This study used analytical tools from the field of complex systems to investigate the stretch-induced collagen reorganization in the human FCL, as an example of a biological material whose loss of structural integrity may lead to changes in tissue mechanics and cellular responses [4,43]. Fibre alignment maps generated using QPLI were converted into weighted collagen

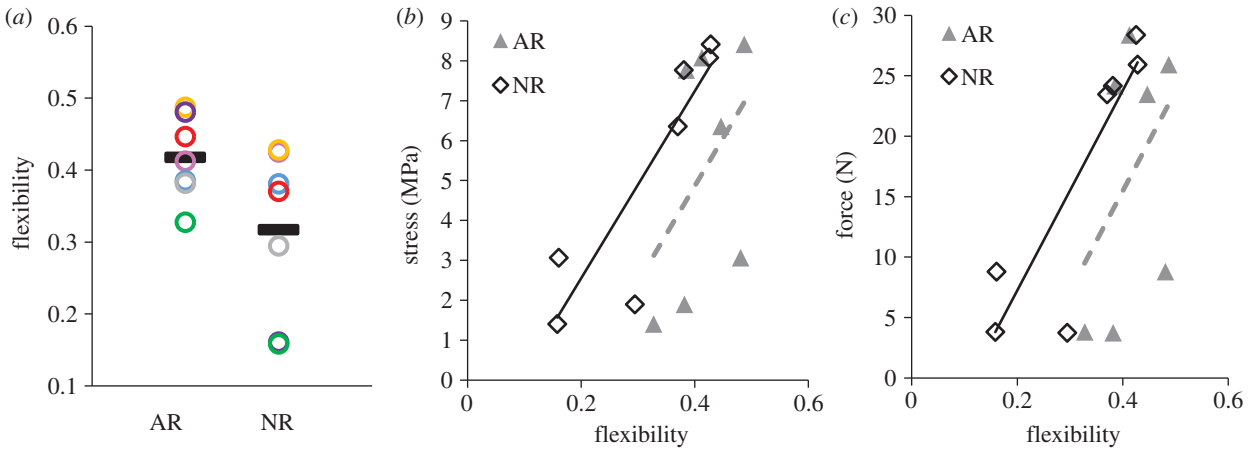


**Figure 4.** Regional differences in flexibility. (*a*) Regions with anomalous realignment (AR) exhibited significantly higher flexibility than normally realigned (NR) regions. Open circles in the same colour represent flexibility from the same FCL sample; black bars indicate the mean flexibility in each region. Correlations between flexibility and (*b*) stress and (*c*) force produced in the FCL at the onset of anomalous realignment were only significant in regions with normal realignment ($R = 0.890$, $p = 0.007$ for stress; $R = 0.877$, $p = 0.010$ for force), but not in regions sustaining anomalous realignment. (Online version in colour.)

alignment networks based on similarity in fibre alignment directions. Community detection methods revealed differences in the modular structure of the constructed collagen networks before and after tensile loading in regions with previously identified anomalous fibre realignment leading to tissue failure (figure 2). Specifically, regions with anomalous fibre realignment, but not regions with normal realignment, exhibited significantly decreased modularity, which was no longer different from that of the null model network, at the onset of atypical fibre realignment compared with the resting state (figure 2). Dynamic community detection on multilayer temporal networks from rest to the onset of anomalous realignment uncovered significantly heightened modular structure with higher stationarity and lower flexibility in the real collagen networks with respect to dynamic null model networks in both AR and NR regions (figure 3), suggesting a smooth and adaptive process of network reorganization during loading. Significant increases in flexibility and loss of correlation between flexibility and FCL mechanics were found in the AR regions compared with NR regions (figure 4), providing evidence of the contribution of local collagen network reorganization to impaired mechanical integrity of the ligament observed at the onset of anomalous fibre realignment.

Here, we have shown network analysis to be a valid method to analyse collagen fibre networks. We demonstrated that regions with anomalous fibre realignment correspond to more evident stretch-induced changes than regions with normal reorganization, consistent with findings based on vector correlation [5,6]. In comparison with prior studies of fibre realignment that largely identified fibre or pixel-level changes [6–8,11], network-based methods provide novel access to *regional* differences in collagen networks' responses to FCL loading. Moreover, this approach provides us new diagnostic variables to characterize the coordinated movement of fibres over time that is evident in the evolution of mesoscale collagen networks. Critically, these tools bridge the features of microscopic tissue injury to the large-scale impairments of macroscopic mechanical integrity.

## 4.1. A stretch-induced decrease in modularity

The finding that local collagen networks of the FCL are modular at rest (figure 2) is consistent with previously reported FCL morphology. Macroscopic and microscopic investigations have revealed that human FCL is composed of irregular connective tissues and parallel bundles of collagenous fibres that run in different directions [2,44]. In the inferior region of the joint, the fibres run in a superior-medial to inferior-lateral direction, whereas in the superior and middle part of the joint, the fibres cross the joint space in the medial-to-lateral direction [44]. This well-organized fibre orientation composed of more than one preferred alignment direction in the FCL is expected to provide heightened modular structures in the collagen networks than random networks as shown using static community detection.

Modularity decreased from rest to the onset of anomalous fibre realignment only in regions that developed atypical fibre reorganization (figure 2). Increases in the mean node degree and average connection strength are potential drivers of the decrease in modularity, as quantitatively confirmed by the significant negative correlations between modularity and both weighted and unweighted average node degrees (electronic supplementary material, figure S1). Thresholding the stretched collagen networks to decrease the number of connections to the resting level while preserving the strongest connections eliminated the difference in modularity between the resting and the stretched states (electronic supplementary material, figure S2), suggesting that loading-induced generation of substantially more weak connections in regions sustaining anomalous fibre realignment plays an important role in collagen network reorganization towards the injury state.

The modular structure of the collagen network at rest was disrupted during stretch of the FCL and underwent a transition to random topology in the regions with anomalous fibre realignment (figure 2). Tensile stretch is known to realign collagen fibres towards the direction of loading [45,46], which is anticipated to decrease the angle differences between collagen bundles aligned in different directions. Substantial fibre realignment with decreasing angle differences during tensile loading can lead to an increase in intermodular connections at the network scale and can result in altered topology, which was qualitatively supported by visualization of the network (figure 2*c*). The structural shift from the modular to random architecture is likely driven by complex topological changes rather than simply an increase in the node degree; collagen networks before and after stretch were both compared quantitatively with their respective null model networks with the same node degree, but exhibited different

structural features. It is important to understand the topological contributions to the altered network architecture, because network-level abnormality may be more detectable and more related to mechanical changes in the macroscale than nodal-level changes.

## 4.2. Dynamic fibre reorganization during loading

Resolving how external loading regulates cellular behaviours is often confounded by dynamic collagen fibre reorganization in the extracellular matrix. Defining the time-dependent fibre kinematics continues to become more feasible due to advancing imaging techniques and computational models [5,7,9,47]. Yet, quantification of coordinated reorganization across spatially distributed fibres over time in real human tissue remains a challenge owing to a lack of analytical tools. In this study, we addressed this challenge using graph-theoretical tools—particularly dynamic community detection of collagen networks—to explore the temporally evolving network architecture of this biological material. Higher stationarity, lower flexibility and heightened modular structure of dynamic collagen networks compared with dynamic network null models indicate the existence of enduring modules, which implies that collagen fibres collectively and smoothly adapt to FCL loading in a coordinated manner. This stretch-induced adaptive realignment of collagen fibres may modulate mechanical behaviours of the FCL as well as other tissues with complex geometry and anatomy, because collagen fibre realignment contributes to the inhomogeneity and nonlinear stress–strain relationships of the material [48].

Mechanical injury events, including material yield or partial failure indicated by a sudden decrease in force with increasing displacement, occurred at the first detection of anomalous realignment for every specimen [5,8]. In addition to those observations at the onset of anomalous realignment, a correlation between tissue forces and flexibility was found only in the NR regions, but not in the AR regions, at the first occurrence of tissue yield and visible rupture that occurred before and after the first detection of atypical reorganization (electronic supplementary material, figure S3). At the eventual gross failure, no correlation was detected between tissue forces and the flexibility measured in either the NR or AR regions (electronic supplementary material, figure S3). The loss of association between FCL mechanical properties and flexibility that occurred before failure in anomalously realigned regions (figure 4) suggests that dynamic changes of mesoscopic collagen networks may contribute to the subfailure impairment of mechanical integrity at the tissue level. The relationships that we found between collagen fibre realignment and the mechanical parameters of the ligament imply a structure–function correlation in the FCL. Anomalous fibre realignment develops at strains significantly lower than those at rupture and predicts the region of visible failure [5]. Because significant differences in flexibility were observed between AR and NR regions from rest to the onset of anomalous realignment, flexibility may be used as a predictor of microstructural abnormality that may lead to eventual ligament failure.

Fibre alignment-based measurements to detect subfailure tissue damage likely have higher sensitivity than the bulk strain measurements. Fibre strains in computationally modelled fibrous networks during uniaxial tensile loading can vary spatially and exceed the applied bulk strain depending on the fibre orientation [49]. The cascade of fibre failure, load redistribution and reorientation of intact fibres that leads to anomalous realignment at the microscale can be complex and non-uniform, particularly considering the structural heterogeneity of the FCL. Therefore, those microscopic changes may not directly align with macroscopic strain measurements. However, the more precise measurements of altered tissue structure instead provide higher resolution to probe tissue impairment in the subfailure regime. In addition, macroscopic tissue strains were typically measured in two-dimensions with surface markers, whereas the QPLI technique captures the average fibre alignment response along the third dimension of the tissue's thickness. Because the FCL is non-uniform through its thickness, alignment-based measurements, such as flexibility, may indeed be more predictive of tissue damage and failure than two-dimensional strains.

## 4.3. Potential application to other materials

This is the first study, to the best of our knowledge, applying graph-theoretical analysis to examine the structural reconfiguration of biological materials. We applied community detection in particular to investigate dynamic collagen fibre reorganization during loading of the human FCL. In addition to the FCL and other capsular ligaments, a variety of other load-bearing tissues in the musculoskeletal system experience collagen reorganization during development, injury and healing [50–52]. Biological soft tissues such as cardiovascular tissue, liver tissue and skin, are also subjected to complex external loading and internal cellular stresses and undergo collagen remodelling in diseased and healing conditions [53–55]. All of those biological systems, which also involve collagen reorganization, could be studied using the graph-theoretical methods introduced here to define dynamic features of this complex multivariate process.

However, the use of network analysis techniques is not limited to natural materials; it could be extended to characterize microstructural reorganization in hydrogels for tissue engineering applications [49,56,57] and to examine dynamic reconfiguration of complex polymer structures [58]. Community detection techniques are highly applicable to studying properties of non-biological materials [24–26] and their use may be expanded in the future to quantitatively investigate physical interactions between material components at intermediate length scales and over time [59–61]. As such, this study provides an advanced framework with quantitative formalisms to investigate dynamic network reorganization that may be applicable to a wide range of complex biological and non-biological materials whose structure may affect bulk material properties and function.

## 4.4. Methodological considerations and future directions

There are several methodological considerations pertinent to this work. First, it remains an open question how to determine some of the input parameters of this technique, such as the pixel window size used to define nodes and the cut-off threshold for establishing connections between nodes. Changes in the input parameters can alter the network size and connection density, which may affect network properties [33]. The parameters used to construct the networks in the current study were chosen based on previously assessed accuracy of the QPLI techniques. Nearby choices of the size of the pixel windows and the cut-off angle threshold varied the network size and density. However, those changes were not

sufficient to alter the finding that the loading-induced changes in modularity only occurred in the AR regions, but not in the NR regions, suggesting that this technique is robust to small variations in input parameters. Nevertheless, systematic testing of the effects of different thresholds would determine the impact of diverse thresholding methods [20,62] and other relevant inputs might have on detecting changes in collagen network structure. Second, there may be additional means for converting the angle differences into edge weights for collagen network construction. In this study, the angle difference was evenly scored from 1 to 10 to generate the connection weights. An alternative is to assign weights based on the probability distribution of the alignment angle difference. Another possible approach is to study the fully weighted network. However, the angle difference still needs to be converted to connection strength as those two quantities are inversely related. More evaluation is required to determine the optimal method for weight assignment. Third, examining the impact of time-step length in the multilayer network formalism would be useful. Future studies could also be conducted to test a broad range of time increments in the multilayer network to evaluate their effects on measuring network dynamics [28].

An alternative approach to quantifying the microstructure of collagen matrix is to use two-point correlation or higher-order correlation functions. The two-point correlation function is a widely used statistic that describes the spatial heterogeneity of the material morphology [63,64]. It defines the distribution of a set of point processes by comparing each point with every other point in the measured space [63,65]. Statistical pair correlation functions are typically computed via analysis of images obtained using confocal, scanning electron microscopy or small X-ray scattering techniques [64,65]. For example, two-point correlation has been used to measure the spatial fluctuations of collagen density and orientation imaged by confocal microscopy during assembly of type I collagen gel [64]. However, the correlation functions capture the probability distribution and cannot uniquely determine the organization of collagen fibre networks (moreover, many different network topologies can be constructed from the same probability distribution). The application of two-point or *N*-point correlation functions to QPLI data for larger-scale collagen configuration requires further investigation.

Although network construction techniques may be further tested and improved in future studies and adjusted for applications on different tissue types, this study demonstrates the relevance and significance of using community detection to define and understand loading-induced collagen reorganization.

## 5. Conclusion

Collagen fibre reorganization plays an important role in cell signalling and tissue homeostasis during loading [5,49]. Because the FCL is a quintessential example of a variety of collagen-based tissues that bridge structural and mechanical changes with altered cellular behaviours, it is important to develop mathematical formalisms accompanying advanced imaging techniques to uncover coordinated collagen fibre movement first in human FCL and to later extend to other biological materials. Using tools from the field of complex systems, we revealed a steady and adaptive transition of the collagen network organization in the FCL from the resting state with heightened modular architecture to the onset of anomalous realignment with random structure. Differences in loading-induced changes in modularity and flexibility between anomalously and normally realigned regions and the loss of association between flexibility and FCL mechanics in regions sustaining anomalous realignment may be used to detect and predict microscopic and macroscopic tissue failure. Our approach provides new insights for understanding how micro- and macroscale tissue mechanics evolve across time and length scales.

Ethics. The post-mortem human subject materials that were analysed in this study were obtained by appropriate guidelines and approved procedures, as previously reported [5].

Data accessibility. Useful open source MATLAB code for network analysis include NetWiki Gen Louvain (http://netwiki.amath.unc.edu/Genlouvain/Genlouvain) and Brain Connectivity Toolbox (https://sites.google.com/site/bctnet/).

Authors' contributions. S.Z., D.S.B. and B.A.W. designed the research and contributed to the writing and editing of the manuscript. S.Z. performed the research implementation, code writing and data analysis. D.S.B. contributed new analytic tools and B.A.W. oversaw all experimental studies generating the original data, the work of S.Z., and also contributed to the interpretation of the data.

Competing interests. The authors declare no competing interests.

Funding. This work was supported by funding from the NIH (U01-EB016638) (B.A.W.), the Alfred P. Sloan Foundation (D.S.B.), the John D. and Catherine T. MacArthur Foundation (D.S.B.) and the NSF (BCS-1430087) (D.S.B.). The content is solely the responsibility of the authors and does not necessarily represent the official views of any of the funding agencies.

Acknowledgement. The authors thank Dr Kyle P. Quinn for performing the experiments that provided the raw QPLI and macromechanics data that were used in these analyses.

## Appendix A

*Modularity* is a quality function used to measure to what extent a given partition of a network compartmentalizes its communities [66,67]. Modularity of a weighted network is defined as

$$Q_{\text{static}} = \frac{1}{2\omega}\sum_{ij}\left(A_{ij} - \frac{k_i k_j}{2\omega}\right)\delta(g_i, g_j),$$

where $A_{ij}$ is the adjacency tensor, $2\omega = \Sigma_{ij} A_{ij}$, $k_i$ is the strength of node $i$, $k_j$ is the strength of node $j$, $\delta$ is the Kronecker delta ($\delta = 1$ for $i$ and $j$ in the same community), $g_i$ is the community to which node $i$ is assigned and $g_j$ is the community to which node $j$ is assigned [35,68]. In this study, modularity is optimized using the Louvain locally greedy algorithm [36].

For the case of temporal networks, the multilayer modularity is defined as

$$Q_{\text{multilayer}} = \frac{1}{2\mu}\sum_{ijlr}\left[\left(A_{ijl} - \gamma_l \frac{k_{il}k_{jl}}{2\omega_l}\right)\delta_{lr} + \delta_{ij}C_{jlr}\right]\delta(g_{il}, g_{jr}),$$

where $A_{ijl}$ is the adjacency tensor between nodes $i$ and $j$ in network slice $l$, $\gamma_l$ is the structural resolution parameter that can be used to tune the size of modules of layer $l$, $k_{il}$ is the strength of node $i$ in layer $l$, $C_{jlr}$ is the connection strength of node $j$ between layer $r$ and layer $l$, $c_{jl} = \Sigma_r C_{jlr}$, $2\mu = \Sigma_{jr}(k_{jr} + c_{jr})$, $g_{il}$ is community $i$ in time slice $l$ and $g_{jr}$ is community $j$ in time slice $r$ [27]. Modularity optimization is performed using a Louvain-like locally greedy algorithm [36].

*Stationarity* is a measure of the mean similarity of module composition over time, calculated as the mean autocorrelation over consecutive time steps. The autocorrelation function

$U(t, t+m)$ of two states of the same community $G(t)$ at $m$ time steps apart is computed using the following formula

$$U(t, t+m) \equiv \frac{|G(t) \cap G(t+m)|}{|G(t) \cup G(t+m)|},$$

where $|G(t) \cap G(t+m)|$ is the number of common nodes in both $G(t)$ and $G(t+m)$, and $|G(t) \cup G(t+m)|$ is the total number of nodes in $G(t)$ and $G(t+m)$ [69]. The stationarity is then defined as

$$\zeta \equiv \frac{\sum_{t=t_0}^{t_f-1} U(t, t+1)}{t_f - t_0 - 1},$$

where $t_0$ is the time when a community emerges, and $t_f$ is the final time step before the given community is extinguished [28,69].

*Flexibility* is a measure of change in the module composition in multilayer networks. Flexibility of node $i$ is defined as

$$f_i = \frac{m}{t_f - 1},$$

where $m$ is the number of times the given node changed modular assignment. The flexibility of the entire network is defined as

$$F = \frac{1}{N} \sum_{i=1}^{N} f_i,$$

where $N$ is the total number of nodes in the network [28].

## References


1. Kallakuri S, Singh A, Lu Y, Chen C, Patwardhan A, Cavanaugh JM. 2008 Tensile stretching of cervical facet joint capsule and related axonal changes. *Eur. Spine J.* **17**, 556–563. (doi:10.1007/s00586-007-0562-0)
2. Kallakuri S, Li Y, Chen C, Cavanaugh JM. 2012 Innervation of cervical ventral facet joint capsule: histological evidence. *World J. Orthop.* **3**, 10–14. (doi:10.5312/wjo.v3.i2.10)
3. Chen C, Lu Y, Kallakuri S, Patwardhan A, Cavanaugh JM. 2006 Distribution of A-delta and C-fiber receptors in the cervical facet joint capsule and their response to stretch. *J. Bone Joint Surg. Am.* **88**, 1807–1816. (doi:10.2106/JBJS.E.00880)
4. Dong L, Quindlen JC, Lipschutz DE, Winkelstein BA. 2012 Whiplash-like facet joint loading initiates glutamatergic responses in the DRG and spinal cord associated with behavioral hypersensitivity. *Brain Res.* **1461**, 51–63. (doi:10.1016/j.brainres.2012.04.026)
5. Quinn KP, Winkelstein BA. 2009 Vector correlation technique for pixel-wise detection of collagen fiber realignment during injurious tensile loading. *J. Biomed. Opt.* **14**, 054010. (doi:10.1117/1.3227037)
6. Quinn KP, Bauman JA, Crosby ND, Winkelstein BA. 2010 Anomalous fiber realignment during tensile loading of the rat facet capsular ligament identifies mechanically induced damage and physiological dysfunction. *J. Biomech.* **43**, 1870–1875. (doi:10.1016/j.jbiomech.2010.03.032)
7. Sander EA, Stylianopoulos T, Tranquillo RT, Barocas VH. 2009 Image-based multiscale modeling predicts tissue-level and network-level fiber reorganization in stretched cell-compacted collagen gels. *Proc. Natl Acad. Sci. USA* **106**, 17 675–17 680. (doi:10.1073/pnas.0903716106)
8. Quinn KP, Winkelstein BA. 2008 Altered collagen fiber kinematics define the onset of localized ligament damage during loading. *J. Appl. Physiol.* **105**, 1881–1888. (doi:10.1152/japplphysiol.90792.2008)
9. Tower TT, Neidert MR, Tranquillo RT. 2002 Fiber alignment imaging during mechanical testing of soft tissues. *Ann. Biomed. Eng.* **30**, 1221–1233. (doi:10.1114/1.1527047)
10. Lee DJ, Winkelstein BA. 2012 The failure response of the human cervical facet capsular ligament during facet joint retraction. *J. Biomech.* **45**, 2325–2329. (doi:10.1016/j.jbiomech.2012.07.015)
11. Quinn KP, Winkelstein BA. 2011 Detection of altered collagen fiber alignment in the cervical facet capsule after whiplash-like joint retraction. *Ann. Biomed. Eng.* **39**, 2163–2173. (doi:10.1007/s10439-011-0316-3)
12. Quinn KP, Winkelstein BA. 2011 Preconditioning is correlated with altered collagen fiber alignment in ligament. *J. Biomech. Eng.* **133**, 064506. (doi:10.1115/1.4004205)
13. Hadi MF, Sander EA, Barocas VH. 2012 Multiscale model predicts tissue-level failure from collagen fiber-level damage. *J. Biomech. Eng.* **134**, 091005. (doi:10.1115/1.4007097)
14. Hodgson RJ, O'Connor PJ, Grainger AJ. 2012 Tendon and ligament imaging. *Br. J. Radiol.* **85**, 1157–1172. (doi:10.1259/bjr/34786470)
15. Hayashi K, Frank JD, Dubinsky C, Zhengling H, Markel MD, Manley PA, Muir P. 2003 Histologic changes in ruptured canine cranial cruciate ligament. *Vet. Surg.* **32**, 269–277. (doi:10.1053/jvet.2003.50023)
16. Newman M. 2010 *Networks: an introduction*. Oxford, UK: Oxford University Press.
17. Ganguly N, Deutsch A, Mukherjee A (eds). 2009 *Dynamics on and of complex networks*. Boston, MA: Birkhäuser Boston. (cited 27 January 2015)
18. Bassett DS, Wymbs NF, Porter MA, Mucha PJ, Grafton ST. 2014 Cross-linked structure of network evolution. *Chaos* **24**, 013112. (doi:10.1063/1.4858457)
19. Zhu X, Gerstein M, Snyder M. 2007 Getting connected: analysis and principles of biological networks. *Genes Dev.* **21**, 1010–1024. (doi:10.1101/gad.1528707)
20. Rubinov M, Sporns O. 2010 Complex network measures of brain connectivity: uses and interpretations. *Neuroimage* **52**, 1059–1069. (doi:10.1016/j.neuroimage.2009.10.003)
21. Kaiser M. 2011 A tutorial in connectome analysis: topological and spatial features of brain networks. *Neuroimage* **57**, 892–907. (doi:10.1016/j.neuroimage.2011.05.025)
22. Meunier D, Achard S, Morcom A, Bullmore E. 2009 Age-related changes in modular organization of human brain functional networks. *Neuroimage* **44**, 715–723. (doi:10.1016/j.neuroimage.2008.09.062)
23. Luscombe NM, Babu MM, Yu H, Snyder M, Teichmann SA, Gerstein M. 2004 Genomic analysis of regulatory network dynamics reveals large topological changes. *Nature* **431**, 308–312. (doi:10.1038/nature02782)
24. Bassett DS, Owens ET, Porter MA, Manning ML, Daniels KE. 2014 Extraction of force-chain network architecture in granular materials using community detection. *Soft Matter* **11**, 2731–2744. (doi:10.1039/C4SM01821D)
25. Bassett DS, Owens ET, Daniels KE, Porter MA. 2012 Influence of network topology on sound propagation in granular materials. *Phys. Rev. E* **86**, 041306. (doi:10.1103/PhysRevE.86.041306)
26. Walker DM, Tordesillas A. 2014 Examining overlapping community structures within grain property networks. In *2014 IEEE Int. Symp. on Circuits and Systems* (*ISCAS*), *1–5 June, Melbourne, Victoria*, pp. 1275–1278.
27. Mucha PJ, Richardson T, Macon K, Porter MA, Onnela J-P. 2010 Community structure in time-dependent, multiscale, and multiplex networks. *Science* **328**, 876–878. (doi:10.1126/science.1184819)
28. Bassett DS, Wymbs NF, Porter MA, Mucha PJ, Carlson JM, Grafton ST. 2011 Dynamic reconfiguration of human brain networks during learning. *Proc. Natl Acad. Sci. USA* **108**, 7641–7646. (doi:10.1073/pnas.1018985108)
29. Lu Y, Chen C, Kallakuri S, Patwardhan A, Cavanaugh JM. 2005 Neurophysiological and biomechanical characterization of goat cervical facet joint capsules. *J. Orthop. Res.* **23**, 779–787. (doi:10.1016/j.orthres.2005.01.002)
30. Gefen A, van Nierop B, Bader DL, Oomens CW. 2008 Strain–time cell-death threshold for skeletal

muscle in a tissue-engineered model system for deep tissue injury. *J. Biomech*. **41**, 2003–2012. (doi:10.1016/j.jbiomech.2008.03.039)

31. Deng B, Begeman PC, Yang KH, Tashman S, King AI. 2000 Kinematics of human cadaver cervical spine during low speed rear-end impacts. *Stapp Car Crash J*. **44**, 171–188.
32. Lee KE, Thinnes JH, Gokhin DS, Winkelstein BA. 2004 A novel rodent neck pain model of facet-mediated behavioral hypersensitivity: implications for persistent pain and whiplash injury. *J. Neurosci. Methods* **137**, 151–159. (doi:10.1016/j.jneumeth.2004.02.021)
33. Van Wijk BCM, Stam CJ, Daffertshofer A. 2010 Comparing brain networks of different size and connectivity density using graph theory. *PLoS ONE* **5**, e13701. (doi:10.1371/journal.pone.0013701)
34. Swingler K. 1996 *Applying neural networks: a practical guide*. San Francisco, CA: Morgan Kaufmann.
35. Newman MEJ. 2006 Modularity and community structure in networks. *Proc. Natl Acad. Sci. USA* **103**, 8577–8582. (doi:10.1073/pnas.0601602103)
36. Blondel VD, Guillaume J-L, Lambiotte R, Lefebvre E. 2008 Fast unfolding of communities in large networks. *J. Stat. Mech. Theory Exp*. **2008**, P10008. (doi:10.1088/1742-5468/2008/10/P10008)
37. Good BH, de Montjoye Y-A, Clauset A. 2010 Performance of modularity maximization in practical contexts. *Phys. Rev. E* **81**, 046106. (doi:10.1103/PhysRevE.81.046106)
38. Fruchterman TMJ, Reingold EM. 1991 Graph drawing by force-directed placement. *Softw. Pract. Exp*. **21**, 1129–1164. (doi:10.1002/spe.4380211102)
39. Kamada T, Kawai S. 1989 An algorithm for drawing general undirected graphs. *Inf. Process. Lett*. **31**, 7–15. (doi:10.1016/0020-0190(89)90102-6)
40. Traud AL, Frost C, Mucha PJ, Porter MA. 2009 Visualization of communities in networks. *Chaos* **19**, 041104. (doi:10.1063/1.3194108)
41. Bassett DS, Porter MA, Wymbs NF, Grafton ST, Carlson JM, Mucha PJ. 2013 Robust detection of dynamic community structure in networks. *Chaos* **23**, 013142. (doi:10.1063/1.4790830)
42. Jutla IS, Jeub LGS, Mucha PJ. 2011–2012 A generalized Louvain method for community detection implemented in MATLAB. See http://arxiv.org/abs/1206.4969.
43. Bogduk N. 2011 On cervical zygapophysial joint pain after whiplash. *Spine* (*Philadelphia, PA. 1976*). **36**, S194–S199. (doi:10.1097/BRS.0b013e3182387f1d)
44. Yamashita T, Minaki Y, Ozaktay AC, Cavanaugh JM, King AI. 1996 A morphological study of the fibrous capsule of the human lumbar facet joint. *Spine* (*Philadelphia, PA. 1976*) **21**, 538–543. (doi:10.1097/00007632-199603010-00002)
45. Lake SP, Barocas VH. 2011 Mechanical and structural contribution of non-fibrillar matrix in uniaxial tension: a collagen–agarose co-gel model. *Ann. Biomed. Eng*. **39**, 1891–1903. (doi:10.1007/s10439-011-0298-1)
46. Vader D, Kabla A, Weitz D, Mahadevan L. 2009 Strain-induced alignment in collagen gels. *PLoS ONE* **4**, e5902. (doi:10.1371/journal.pone.0005902)
47. Wang H, Nair A, Chen CS, Wells RG, Shenoy VB. 2014 Long range force transmission in fibrous matrices enabled by tension-driven alignment of fibers. *Biophys. J*. **107**, 2592–2603. (doi:10.1016/j.bpj.2014.09.044)
48. Lake SP, Miller KS, Elliott DM, Soslowsky LJ. 2009 Effect of fiber distribution and realignment on the nonlinear and inhomogeneous mechanical properties of human supraspinatus tendon under longitudinal tensile loading. *J. Orthop. Res*. **27**, 1596–1602. (doi:10.1002/jor.20938)
49. Zhang S, Cao X, Stablow AM, Shenoy VB, Mechanics A, Winkelstein BA. 2015 Tissue strain reorganizes collagen with a switch-like response that regulates neuronal ERK phosphorylation *in vitro*: implications for ligamentous injury & mechanotransduction. *J. Biomech. Eng*. (doi:10.1115/1.4031975)
50. Sharma P, Maffulli N. 2006 Biology of tendon injury: healing, modeling and remodeling. *J. Musculoskelet. Neuronal Interact*. **6**, 181–190.
51. Provenzano PP, Vanderby R. 2006 Collagen fibril morphology and organization: implications for force transmission in ligament and tendon. *Matrix Biol*. **25**, 71–84. (doi:10.1016/j.matbio.2005.09.005)
52. Van Turnhout MC, Kranenbarg S, van Leeuwen JL. 2011 Contribution of postnatal collagen reorientation to depth-dependent mechanical properties of articular cartilage. *Biomech. Model. Mechanobiol*. **10**, 269–279. (doi:10.1007/s10237-010-0233-7)
53. Hariton I, de Botton G, Gasser TC, Holzapfel GA. 2007 Stress-driven collagen fiber remodeling in arterial walls. *Biomech. Model. Mechanobiol*. **6**, 163–175. (doi:10.1007/s10237-006-0049-7)
54. Verhaegen PD, Schouten HJ, Tigchelaar-Gutter W, van Marle J, van Noorden CJ, Middelkoop E, van Zuijlen PP. 2012 Adaptation of the dermal collagen structure of human skin and scar tissue in response to stretch: an experimental study. *Wound Repair Regen*. **20**, 658–666. (doi:10.1111/j.1524-475X.2012.00827.x)
55. Cox TR, Erler JT. 2011 Remodeling and homeostasis of the extracellular matrix: implications for fibrotic diseases and cancer. *Dis. Model. Mech*. **4**, 165–178. (doi:10.1242/dmm.004077)
56. Parenteau-Bareil R, Gauvin R, Berthod F. 2010 Collagen-based biomaterials for tissue engineering applications. *Materials* (*Basel*). **3**, 1863–1887. (doi:10.3390/ma3031863)
57. Nagel T, Kelly DJ. 2012 Remodelling of collagen fibre transition stretch and angular distribution in soft biological tissues and cell-seeded hydrogels. *Biomech. Model. Mechanobiol*. **11**, 325–339. (doi:10.1007/s10237-011-0313-3)
58. Chomakova-Haefke M, Nyffenegger R, Schmidt E. 1994 Structure reorganization in polymer films of nafion due to swelling studied by scanning force microscopy. *Appl. Phys. A Solids Surfaces* **59**, 151–153. (doi:10.1007/BF00332208)
59. Kramár M, Goullet A, Kondic L, Mischaikow K. 2014 Evolution of force networks in dense particulate media. *Phys. Rev. E* **90**, 052203. (doi:10.1103/PhysRevE.90.052203)
60. Walker DM, Tordesillas A. 2012 Taxonomy of granular rheology from grain property networks. *Phys. Rev. E* **85**, 011304. (doi:10.1103/PhysRevE.85.011304)
61. Herrera M, McCarthy S, Slotterback S, Cephas E, Losert W, Girvan M. 2011 Path to fracture in granular flows: dynamics of contact networks. *Phys. Rev. E* **83**, 061303. (doi:10.1103/PhysRevE.83.061303)
62. Lohse C, Bassett DS, Lim KO, Carlson JM. 2014 Resolving anatomical and functional structure in human brain organization: identifying mesoscale organization in weighted network representations. *PLoS Comput. Biol*. **10**, e1003712. (doi:10.1371/journal.pcbi.1003712)
63. Jiao Y, Stillinger FH, Torquato S. 2007 Modeling heterogeneous materials via two-point correlation functions: basic principles. *Phys. Rev. E* **76**, 031110. (doi:10.1103/PhysRevE.76.031110)
64. Jones CAR, Liang L, Lin D, Jiao Y, Sun B. 2014 The spatial-temporal characteristics of type I collagen-based extracellular matrix. *Soft Matter* **10**, 8855–8863. (doi:10.1039/c4sm01772b)
65. Baniassadi M, Ahzi S, Garmestani H, Ruch D, Remond Y. 2012 New approximate solution for N-point correlation functions for heterogeneous materials. *J. Mech. Phys. Solids* **60**, 104–119. (doi:10.1016/j.jmps.2011.09.009)
66. Porter MA, Onnela J-P, Mucha PJ. 2009 Communities in networks. *Not. Am. Math. Soc*. **56**, 1082–1097.
67. Fortunato S. 2010 Community detection in graphs. *Phys. Rep*. **486**, 75–174. (doi:10.1016/j.physrep.2009.11.002)
68. Newman M. 2004 Fast algorithm for detecting community structure in networks. *Phys. Rev. E* **69**, 066133. (doi:10.1103/PhysRevE.69.066133)
69. Palla G, Barabási A-L, Vicsek T. 2007 Quantifying social group evolution. *Nature* **446**, 664–667. (doi:10.1038/nature05670)